



NUMERICAL INVESTIGATION OF THE FLUID-STRUCTURE INTERACTION IN 2-D FLOW OVER A CYLINDER

Rafael Nascimento Ihi

Luiz Augusto C. A. Schiavo

João Henrique A. Azevedo

Instituto Tecnológico de Aeronáutica, DCTA/ITA, Brazil

rafael.ihl@hotmail.com, augustoschiavo@gmail.com, joaohenrique.azevedo@gmail.com

João Luiz F. Azevedo

Instituto de Aeronáutica e Espaço, DCTA/IAE/ALA, Brazil

joaoluiz.azevedo@gmail.com

Abstract. Problems of fluid-structure interaction are of practical interest in several areas of engineering. The vortex-induced vibration (VIV) phenomenon can be found in launch vehicles at the launch pad, transmission lines and risers used in prospecting and exploration of oil in the oceans, among others. The prediction of this phenomenon is critical to the success of the corresponding applications. The long term objective of the work here reported is to develop the capability of analyzing fluid-structure interaction problems on oil-platform risers using CFD techniques. Thus, the specific research included here aims to analyze the physical phenomena present in the wake of cylinders at different Reynolds numbers, as well as their effects on the bodies present in the flow. Tests are performed with fixed cylinders and moving cylinders. In the second case, both the situations in which the movement is prescribed and situations in which the cylinder is free to move under the forces acting upon the body are analyzed. In the latter case, the cylinder is restrained by linear springs which have their stiffness constants calculated in such a way to yield natural oscillating frequencies that correspond to representative oscillating frequencies found in practice. The flows of interest are assumed to be adequately modeled by the 2-D Reynolds-averaged Navier-Stokes (RANS) equations, with appropriate turbulence closures. The flow Reynolds number, based on the cylinder diameter, is varied from 300 to 10,000. The results are compared to the available data and show good agreement. However, it is observed that the 2-D simulations are not adequate for the practical applications of interesting.

Keywords: Vortex induced vibration, Fluid-structure interaction, CFD, Free and forced oscillations

1. INTRODUCTION

Vortex-induced vibration (VIV) is a particular case of the fluid-structure interaction phenomenon that affects many fields of engineering and has been the subject of a large number of investigations, such as the work of Sarpkaya (1979), Griffin and Ramberg (1982), Blevins (1990) and Williamson (1996). So far, there is a larger availability of data for low Reynolds numbers (Re), while, for higher values of this parameter, it becomes increasingly more difficult to find reliable data. One of the most studied cases of VIV is the flow around a free cylinder, due to its practical applications concerning the dynamics of oil risers, chimney towers, high voltage cables and antennae, among others. The asymmetry of the vortex shedding by the immersed body induces the structure's vibration which, consequently, influences the vortex shedding. The flow for $Re < 49$ is steady with symmetric vortex formation around the wake center line. Above $Re = 49$, the onset of the laminar vortex shedding is observed, forming the von Karman vortex street. For $Re > 260$, vortices start to develop in the spanwise direction of the cylinder, and the flow gradually loses its two-dimensional characteristics (Williamson, 1996).

The first lift measurement on a circular cylinder was carried out by Drescher (1956), who recorded the wall pressure around an underwater cylinder with a Reynolds number of 110,000. Recent efforts to predict the lift and drag coefficients of an oscillating cylinder under prescribed displacement, using numerical simulations were made by Lima e Silva *et al.* (2003) and Dong and Karniadakis (2005), the latter using direct numerical simulation (DNS). There is also experimental data from Norberg (2003). Nonetheless, the literature lacks lift and drag measurements for a freely vibrating cylinder, with few exceptions, such as in the review of Khalak and Williamson (1999), who conducted a two degree of freedom experiment for a Reynolds number around 6000.

The present work is focused on the numerical investigation of the fluid-structure interaction of a flow over a cylinder, and the validation of a CFD tool through the comparison between the aerodynamic coefficients of an oscillating circular cylinder and results of the literature, some of which are mentioned above. The cylinder is considered to be elastically mounted and rigid, undergoing either forced or free oscillation. In the former case, the body is restrained to move transversely or longitudinally to the flow, by a prescribed harmonic displacement of moderate amplitude. In the latter case, the cylinder is free to move only in the crossflow direction and its motion is governed by a structural-dynamic

equation. Moreover, the influence of Reynolds number and flow velocity on the aerodynamic coefficients of the cylinder are analyzed.

2. NUMERICAL FORMULATION

The CFD tool used in this work is based on the 2-D Navier-Stokes equations, which represent a two dimensional flow of compressible viscous fluid through a continuous medium in transient regime. In a finite volume approach, these equations can be written in Cartesian form as

$$\frac{\partial}{\partial t} \int_{V_i} Q dx dy + \oint_{S_i} (E dy - F dx) = 0. \quad (1)$$

In Eq. (1), V represents the control volume or the area, and S is the length of the edges of the element. The Q variable is a vector of conserved properties, and the E and F variables are the flux vectors in the x and y directions, respectively. These variables are written as

$$Q = [\rho \quad \rho u \quad \rho v \quad e]^T, \quad (2)$$

$$E = E_e + E_v \quad \text{and} \quad F = F_e + F_v. \quad (3)$$

Here, E_e and F_e represent the inviscid flux, or Euler flux, and E_v and F_v represent the viscous terms. The Euler fluxes are

$$E_e = \left\{ \begin{array}{c} \rho U_c \\ \rho u U_c + p \\ \rho v U_c \\ (e + p) U_c + x_t p \end{array} \right\}, \quad F_e = \left\{ \begin{array}{c} \rho V_c \\ \rho u V_c \\ \rho v V_c + p \\ (e + p) V_c + y_t p \end{array} \right\}. \quad (4)$$

In the previous equations, U_c and V_c are the contravariant velocity components, which, in unsteady cases, take into account the mesh velocity components x_t and y_t as

$$U_c = u - x_t, \quad V_c = v - y_t. \quad (5)$$

The viscous flux vectors are written as

$$E_v = \left\{ \begin{array}{c} 0 \\ \tau_{ii} \\ \tau_{ji} \\ \tau_{ii} u + \tau_{ji} u - q_j \end{array} \right\}, \quad F_v = \left\{ \begin{array}{c} 0 \\ \tau_{ij} \\ \tau_{jj} \\ \tau_{ij} v + \tau_{jj} v - q_j \end{array} \right\}. \quad (6)$$

The nomenclature employed here is usual in the CFD community, where ρ is density or specific mass, u and v are the Cartesian velocity components in the x and y directions, respectively, e is the total energy, p is the pressure, τ_{ij} are the components of the viscous stress tensor in Einstein's notation, μ is the molecular dynamic viscosity coefficient, δ_{ij} is the Kronecker delta operator, and λ is the volumetric viscosity coefficient which is defined by the Stokes hypothesis. As such, τ_{ij} and λ are written as

$$\tau_{ij} = \mu \left(\frac{\partial u_i}{\partial x_j} + \frac{\partial u_j}{\partial x_i} \right) + \lambda \frac{\partial u_k}{\partial x_k} \delta_{ij}, \quad \lambda = -\frac{2}{3} \mu. \quad (7)$$

Finally, the heat flux, q_i , is obtained by Fourier's law of heat conduction, where K is the coefficient of thermal conductivity.

$$q_i = -K \frac{\partial T}{\partial x_i}. \quad (8)$$

2.1 Spatial Discretization

The numerical scheme adopted in this work is a cell centered finite volume method. The discrete value of conserved flow field vector variables is computed for the i -th control volume as

$$Q_i = \frac{1}{V} \int_{V_i} Q dV, \quad (9)$$

where Q_i is the mean value of Q in the instant of time t , for the control volume V_i . Equation (1) can be rewritten for each i th cell as

$$\frac{\partial Q_i}{\partial t} = - \int_{S_i} (E dy - F dx). \quad (10)$$

According to Mavriplis (1990), for each control volume face, flux information of flow field variables must be computed from i -th and n_b -th control volumes which share a k -th face. Hence, the flux computation is built as

$$\int_{s_i} (E dy - F dx) \approx \sum_{k=1}^{s_i} [E(Q_k)(y_2 - y_1) - F(Q_k)(x_2 - x_1)] . \quad (11)$$

The $E(Q_k)$ and $F(Q_k)$ fluxes are computed by a prescribed value, Q_k , at the k -th face. The flux computation is, then, accordingly distributed between i -th and n_b -th control volumes. Moreover, all variables or parameters necessary at face are computed by a simple averaged procedure,

$$Q_k = \frac{1}{2}(Q_i + Q_{n_b}) . \quad (12)$$

Thus, the inviscid and viscous fluxes can be written for each control volume as

$$C(Q_i) = \sum_{k=1}^{nf} [E_e(Q_k)(y_2 - y_1) - F_e(Q_k)(x_2 - x_1)] , \quad (13)$$

$$V(Q_i) = \sum_{k=1}^{nf} [E_v(Q_k)(y_2 - y_1) - F_v(Q_k)(x_2 - x_1)] . \quad (14)$$

$D(Q_i)$ is the algebraic artificial dissipation operator proposed by Mavriplis (1990) as

$$D(Q_i) = \xi_{i,n_b}^2 d^2(Q_i) - \xi_{i,n_b}^4 d^4(Q_i) . \quad (15)$$

2.2 Time Discretization

The second-order accurate, five-stage, explicit hybrid Runge-Kutta scheme proposed by Jameson and Mavriplis (1986) and by Batina (1991) is adopted for the time discretization. This scheme can be written as

$$\begin{aligned} Q_i^{(0)} &= Q_i^n , \\ Q_i^{(j)} &= \frac{V_i^n}{V_i^{n+1}} Q_i^{(0)} - \Theta_j \frac{\Delta t_i}{V_i^{n+1}} [C(Q_i^{(j-1)}) - D(Q_i^{(j-1)}) - V(Q_i^{(0)})] , \\ Q_i^{n+1} &= Q_i^{(5)} , \end{aligned} \quad (16)$$

Although the present work considers a mesh moving rigidly with the body, this scheme already includes the necessary terms to account for changes in cell area due to deformation of the mesh (Batina, 1991). The n and $n + 1$ superscripts indicate property values at the beginning and the end of the n -th time step, respectively. The values used for the Θ_j coefficients, as suggested by Mavriplis (1990), are

$$\Theta_1 = \frac{1}{4} , \quad \Theta_2 = \frac{1}{6} , \quad \Theta_3 = \frac{3}{8} , \quad \Theta_4 = \frac{1}{2} , \quad \Theta_5 = 1 . \quad (17)$$

In Eq. (16), the convective operator, C , is evaluated at every stage of the integration process, but the artificial dissipation operator, D , is only evaluated at odd stages. The viscous term, V , is computed only in the first stage and it is kept constant throughout the remaining stages of the Runge-Kutta scheme. This is done with the objective of saving computational time because the evaluation of the latter is rather expensive. As discussed by Jameson *et al.* (1981), this type of procedure is known to provide adequate numerical damping characteristics while achieving the desired reduction in computational cost.

2.3 Turbulence Model and Meshing Considerations

As previously discussed, the structural model considered in the present work is a 2-D cylinder section, which is widely known and reported in the literature. The cases are simulated as both laminar and turbulent flows, given that the current test cases are in the beginning of the laminar to turbulent transition. When running a turbulent case, the Spalart-Allmaras turbulence model (Spalart and Allmaras, 1994) is used. It is implemented in the solver in accordance to the formulation presented in Spalart and Allmaras (1994). That requires less computational efforts to be solved because, by construction, less refined meshes are required near wall surfaces than compared to the more stringent mesh needs for some two equations models. Naturally, the meshes employed for turbulent simulations are much more refined than those used for laminar computations. The meshes used in the present work are generated with the ICFM CFD[®] commercial grid generator. As an example, Fig. 1 shows two views of the laminar mesh around the cylinder section.

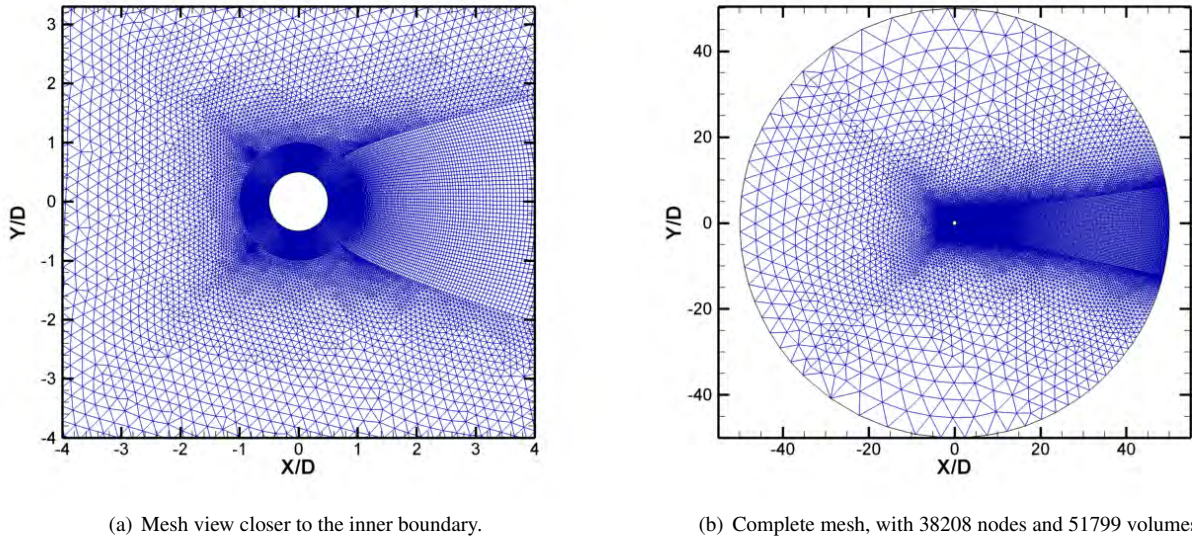


Figure 1. RANS solver mesh around 2-D cylinder section.

The dynamic system represented in the cylinder section is a rigid body with a plunge degree of freedom, transversal to the flow. Unsteady calculations involve body motion and, therefore, the computational mesh and boundary conditions should be somehow adjusted to take this motion into account. Two approaches are adopted here in order to create such movement. The first approach is to prescribe the motion as part of the input of the simulation. Prescribed motions consist of sinusoidal functions. The idea of this approach is to validate the numerical solver through frequency content analysis. On the other hand, the second method is to integrate a structural-dynamic formulation coupled to the fluid dynamics solver. In the present free cylinder model, the stiffness of the beam-like cylinder is represented by a linear spring. The dynamics of the mass-spring system with a natural frequency ω can, then, be written as

$$\frac{d^2 \bar{y}}{dt^2} + \left(\frac{\omega}{\omega_r} \right)^2 \bar{y} = \frac{2C_L}{\pi \mu_r}. \quad (18)$$

Moreover, μ_r is the mass ratio and ω_r is a reference frequency conveniently selected. The previous equation is, then, marched in time using a four-stage Runge-Kutta method which can be written as

$$\begin{aligned} \{y\}_{rk1}^n &= [A] \{y\}^n + \{Q\} \\ \{y\}_{rk2}^n &= [A] \left(\{y\}^n + \frac{\Delta t_s}{2} \{y\}_{rk1}^n \right) + \{Q\} \\ \{y\}_{rk3}^n &= [A] \left(\{y\}^n + \frac{\Delta t_s}{2} \{y\}_{rk2}^n \right) + \{Q\} \\ \{y\}_{rk4}^n &= [A] \left(\{y\}^n + \Delta t_s \{y\}_{rk3}^n \right) + \{Q\} \\ \{y\}^{n+1} &= \{y\}^n + \frac{\Delta t_s}{6} \left(\{y\}_{rk1}^n + 2 \{y\}_{rk2}^n + 2 \{y\}_{rk3}^n + \{y\}_{rk4}^n \right). \end{aligned} \quad (19)$$

Here, $[A]$ and $\{Q\}$ represent the system dynamic matrix and forcing vector, respectively, when the problem is formulated in state space. Finally, the far-field boundary conditions are adjusted in order to account for the motion as reported in Marques and Azevedo (2008). In the present work, the authors have selected to move the mesh rigidly with the inner boundary. This approach is less computationally expensive than employing a deformable mesh, with a fixed outer boundary, that accommodates for the movement of the inner boundary. However, one must bare in mind that the present approach is not as general as the aforementioned deformable mesh procedure, since it can only be used when the structural modes involve rigid body motions, as in the present case. Regardless of the type of motion being calculated, the mesh velocity components can be calculated as

$$\begin{aligned} x_{t_j} &= \frac{x_j^{n+1} - x_j^n}{\Delta t} \\ y_{t_j} &= \frac{y_j^{n+1} - y_j^n}{\Delta t}. \end{aligned} \quad (20)$$

The new cell areas are determined employing the geometric conservation law concept (Thomas and Lombard, 1979), where the total area conservation is imposed in a similar manner to the other flow conserved variables.

3. RESULTS AND DISCUSSION

3.1 Fixed Cylinder Analysis

The initial tests performed consider a fixed cylinder with the purpose of evaluating the accuracy of the present formulation in the analysis of a low Reynolds number flow. Tests are performed at a $Re = 300$ flow, where the Reynolds number is defined in terms of the cylinder diameter. Results for the drag coefficient are compared with the literature as shown in Table 1. The data in Table 1 include the results of Mittal and Balachandar (1997), which brings experimental data, and of Lima e Silva *et al.* (2003), which performed DNS calculations for the same configuration. The other data included in Tab. 1 are extracted from Lima e Silva *et al.* (2003).

Table 1. Mean drag coefficients for a Reynolds number 300 flow over a circular cylinder.

Present work	Lima e Silva et al.	Park et al.	Sucker e Brauer	Ye et al.	Mittal e Balachandar
1.20	1.27	1.37	1.22	1.38	1.22

Another test, performed at a Reynolds number of 1000, has results compared to literature data in Tab. 2. Strouhal number, S_t , lift coefficient, C_L , and mean and maximum drag coefficients, calculated in the present work, are compared to a two-dimensional compressible RANS simulation (Rohde, 2011). All properties analyzed have good correlation with the literature data. It is important to notice that Rohde (2011) used a formulation that is similar to the present work. The cited paper solves the compressible, viscous, two dimensional Navier-Stokes equations without turbulent modeling as in the present case.

Table 2. Aerodynamic properties for the flow over a circular cylinder at $Re = 1000$.

Propriety	Reference	Present Work	Difference (%)
C_ℓ	1.365	1.364	0.1
$C_{d\text{mean}}$	1.462	1.414	3.3
Ampl. C_d	0.188	0.185	1.5
$C_{d\text{max}}$	1.652	1.599	3.2
$S_{t\text{calc.}}$	0.239	0.235	1.8

3.2 Prescribed Motion Analysis

In order to validate the mesh motion algorithm, the results of prescribed motion in the transversal direction, with a moderate amplitude of 0.3 diameters, are compared to the commercial software CFD++[®]. Both cases are simulated with dimensionless frequency $(f_0 d)/U = 0.14$ and Reynolds number $Re = 1000$. A prescribed sinusoidal motion, given by $Y(t) = A \sin(2\pi f_0 t)$, is imposed to the cylinder. Table 3 shows the values of the r.m.s. (root mean square) lift and mean drag obtained. It is observed that the maximum error is only 7%, which demonstrates the good accuracy of the results. As the lift and drag coefficients undergo large changes in time, these coefficients are converted to the frequency domain, through the fast Fourier transform (FFT). The comparison of the magnitude and the frequency content of the unsteady lift and drag coefficients, for both CFD tools, can be visualized in Fig. 2. As noticed from this figure, the corresponding coefficient results show a very good correlation between the solutions with the two different codes. In other words, the spectra of lift and drag coefficients are in good agreement.

Once the mesh motion algorithm is validated, several tests for prescribed motion are performed. The tests consider different frequencies for a fixed Reynolds number of 10,000. As $Re = 10,000$ lies in the transition range, the simulations are carried out not only with a laminar model but also with the turbulence model of Spalart and Allmaras (1994). These test cases, as well as their results, are summarized in Tab. 4. The present results are compared to the DNS data of Dong and Karniadakis (2005) and the empirical results of Gopalkrishnan (1993) in Fig. 3. As expected, the results using the turbulence model are considerably nearer to the reference than the laminar results, for most cases. It can be noticed that the drag coefficients for the laminar and turbulent model are slightly over-predicted and the lift coefficients are under-

R.N. Ihi, L.A.C.A. Schiavo, J.H.A. Azevedo, and J.L.F. Azevedo
 Numerical Investigation of the Fluid-structure Interaction in 2-D Flow Over a Cylinder

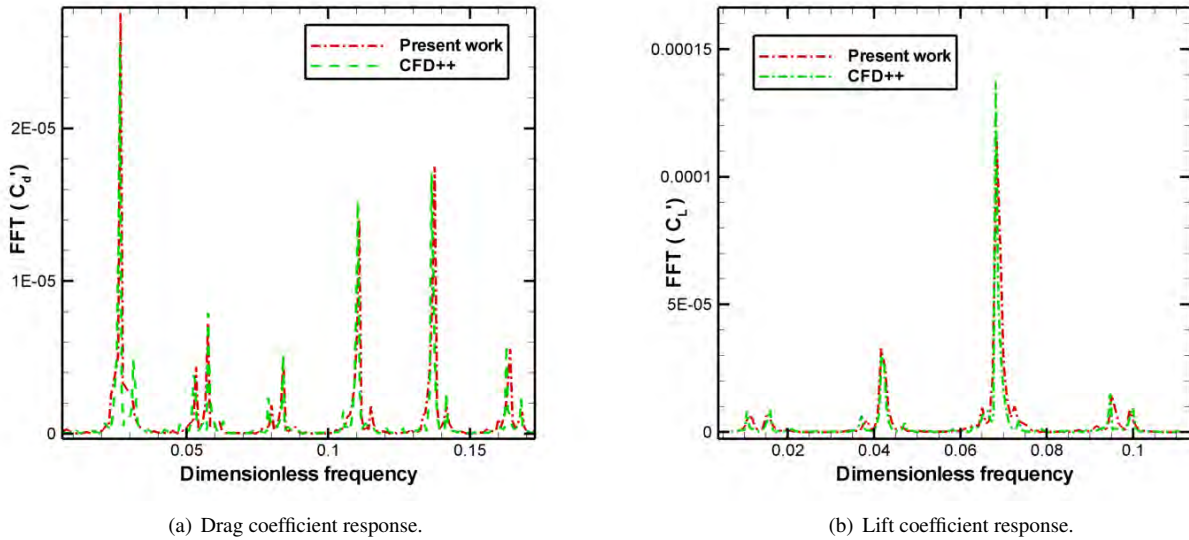


Figure 2. Frequency content of the aerodynamic coefficients for a $Re = 1000$ flow over a cylinder with prescribed motion.

Table 3. Comparison of aerodynamic coefficients for the prescribed motion test case for a $Re = 1000$ flow over a cylinder.

Coefficient	In-house Code	CFD++	Difference (%)
$C_{d\text{mean}}$	1.478	1.594	7
$C_{l\text{rms}}$	0.985	1.034	5

predicted for the highest frequencies. Overall, the results are reasonably close to the literature, with the exception of the M2 case. A possible reason for this behavior is that the frequency for the M2 case is in a range of frequencies that go through a sharp increase in the coefficients and are, therefore, more susceptible to error. Moreover, the present work performs 2-D simulations while the cited references use 3-D configurations. Wu *et al.* (1996) indicate that the onset of 3-D instabilities, such as vortex formation in the spanwise direction, occurs for $Re > 200$. As indicated, these 3-D effects are not accounted for in the present work. A few simulations with forced oscillation in the transverse direction are also

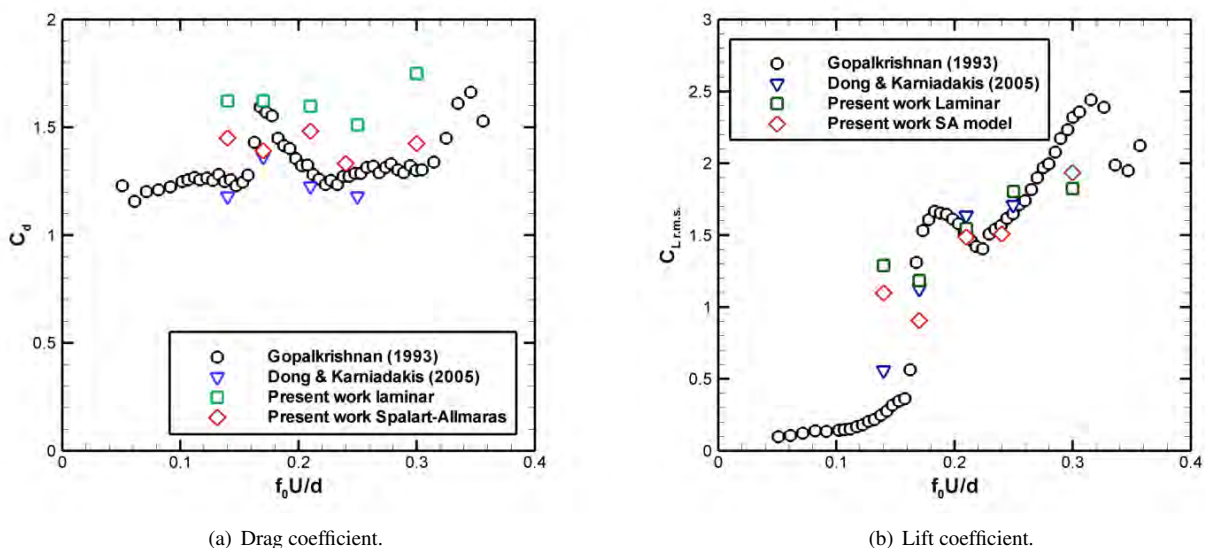


Figure 3. Comparison of the aerodynamic coefficients for a prescribed cylinder oscillation at $Re = 10,000$.

conducted in order to demonstrate the capability of the code to allow for oscillations in this direction as well. The results

Table 4. Transversal oscillation results.

Case	Re	Amplitude (Y/d)	f_0U/d	$C_{d,mean}$	$C_{\ell,rms}$
M1	1,000	0.3	0.14	1.478	0.985
M2	10,000	0.3	0.14	1.623	1.288
M3	10,000	0.3	0.17	1.624	1.184
M4	10,000	0.3	0.21	1.598	1.546
M5	10,000	0.3	0.25	1.511	1.804
M6	10,000	0.3	0.30	1.750	1.825

are shown in Tab. 5.

Table 5. Longitudinal oscillation results.

Case	Re	Amplitude (X/d)	f_0U/d	$C_{d,mean}$	$C_{\ell,rms}$
M7	10,000	0.1	0.05	1.698	1.308
M8	10,000	0.1	0.10	1.733	1.329
M9	10,000	0.1	0.15	1.635	1.241

3.3 Free Motion Analysis

The simulations for free motion are conducted in such a way that, initially, calculations are performed for a fixed cylinder until the aerodynamic solution reaches a periodic state. This state provides the initial condition for the free cylinder calculations. Then, the cylinder is allowed to oscillate in the transversal direction by the influence of the aerodynamic forces. From this point on, the structure is considered to be constrained by linear springs in order to model the cylinder stiffness. The frequency response ratio is defined as

$$f^* = \frac{f}{f_n}, \quad (21)$$

where f is the body oscillation frequency. The reduced velocity is expressed by

$$U^* = \frac{2\pi U}{f_n d}, \quad (22)$$

where d is the cylinder diameter and, in both equations, f_n is the natural frequency of the structure. Since the freestream flow velocity, U , is constant, as are most of the terms in Eq. (22), the only free parameter is the natural frequency, which in turn is a function of the spring stiffness.

Figure 4 (a) illustrates the behavior of the frequency response ratio, f^* , as a function of the reduced velocity, U^* . The results are indicating that, with the increase of reduced velocity, the vortex shedding frequency becomes closer to the natural frequency of the system and, hence, the two frequencies synchronize. This is the well known definition of the lock-in phenomenon (Williamson and Govardhan, 2004). The onset of the lock-in is characterized by a resonance and a hysteresis which was first demonstrated by Feng (1968). As illustrated in Fig. 4 (b), in the lock-in region, the amplitude undergoes a sharp increase. The behavior of f^* in the synchronization regime is similar to what is reported in the experimental work of Khalak and Williamson (1999) for low mass ratios. The results for dimensionless amplitude, $A^* = A_{max}/d$, as a function of the reduced velocity, are compared in Fig. 4 (b) to 2-D and 3-D DNS and experimental results obtained by Blackburn *et al.* (2000). Three response branches are clearly observed from this plot: the initial excitation, the upper and the lower branches.

The initial excitation branch is characterized by an intense growth ratio which quickly reaches the highest values of A^* in the upper branch. The third (lower) branch displays a more moderate behavior in which the amplitude slowly decreases as U^* is incremented. There is also an abrupt change in the phase angle between the lift force and the body displacement, ranging from approximately 0° from the previous modes to 180° . Both the experimental data and the 3-D simulation results exhibit reasonable correlation, differently from the 2-D ones. Although one expects certain discrepancies between 2-D and 3-D simulations, because of the aforementioned three-dimensional effects, the difference observed is much more significant than anticipated. This fact is also corroborated by Tab. 6 that shows peak amplitude data for 2-D, 3-D and

empirical tests, made by various authors. The peak amplitudes obtained in 2-D simulations are substantially under-predicted when compared to the three-dimensional calculation results, as well as being incapable of accurately estimating the response branches.

Figure 4 (b) also shows that there is good agreement between the 2-D results of Blackburn *et al.* (2000) and the present work, especially in the range $4.5 < U^* < 6.5$. Although the agreement between the results is not as good in the $3 < U^* < 4$ range, it is fair to state that there is good overall correlation between the 2-D results. It is noteworthy to emphasize that Blackburn *et al.* (2000) performed DNS calculations, while the present work is based on the RANS equations with the Spalart and Allmaras (1994) turbulence model. It is known that the RANS formulation is not very effective to simulate flows in the laminar-turbulent transition regime, especially when there is a large region with a separated flow. RANS turbulence models typically consider the flow either fully turbulent or laminar, and this does not yield a good approximation in the transition regime. For this reason, a certain error is expected in these results.

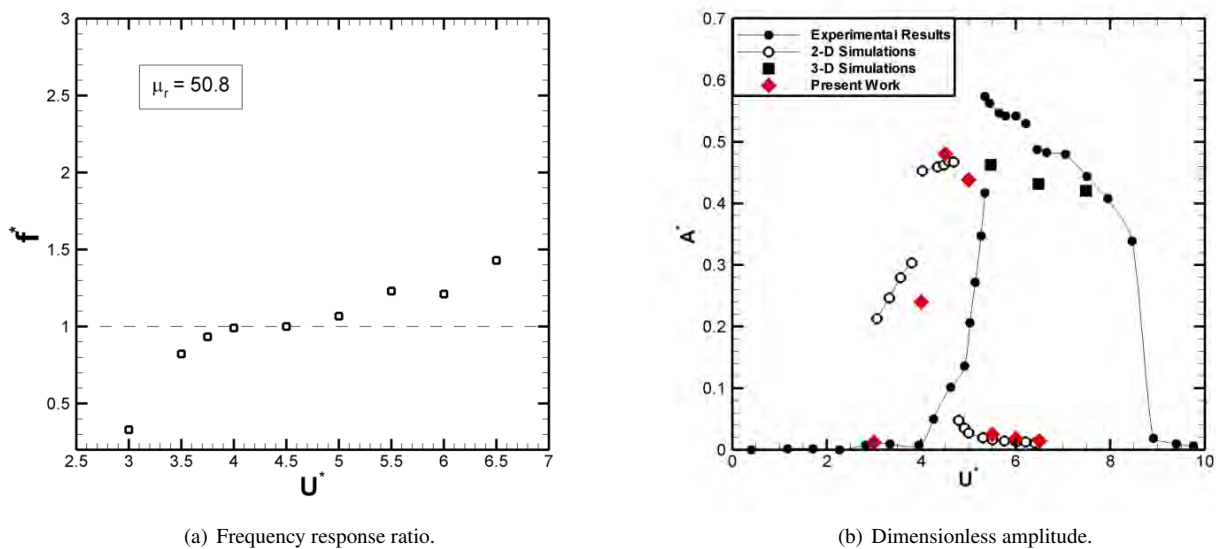
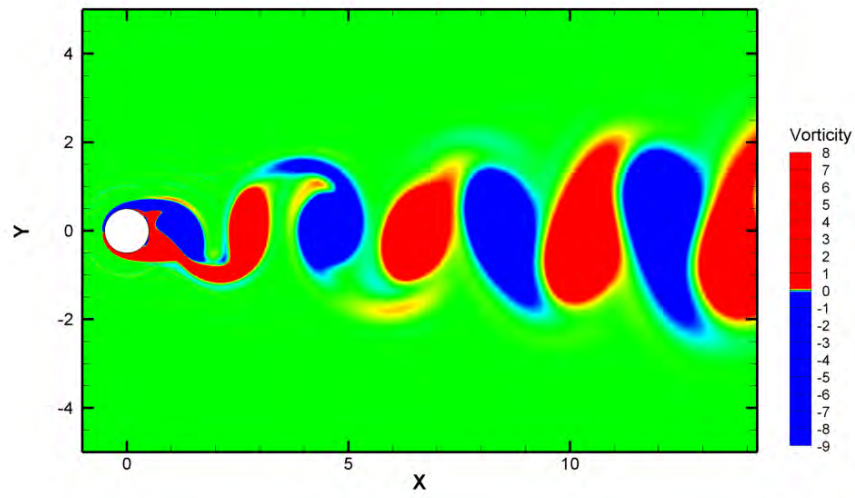
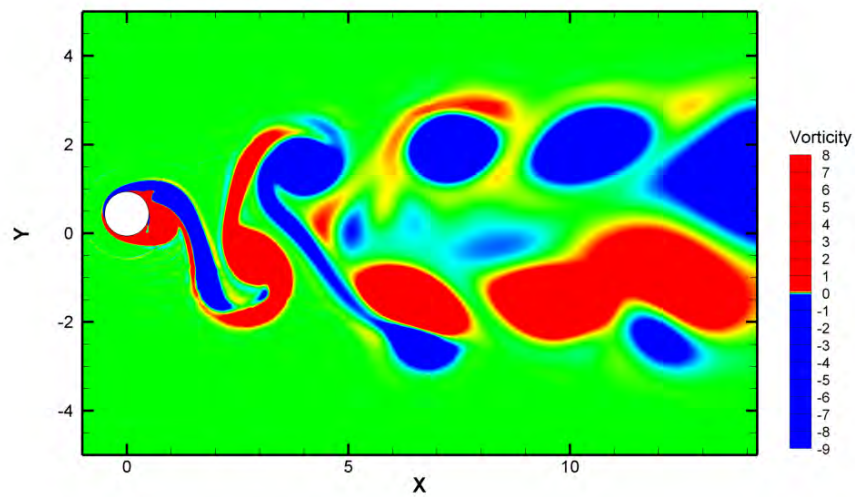
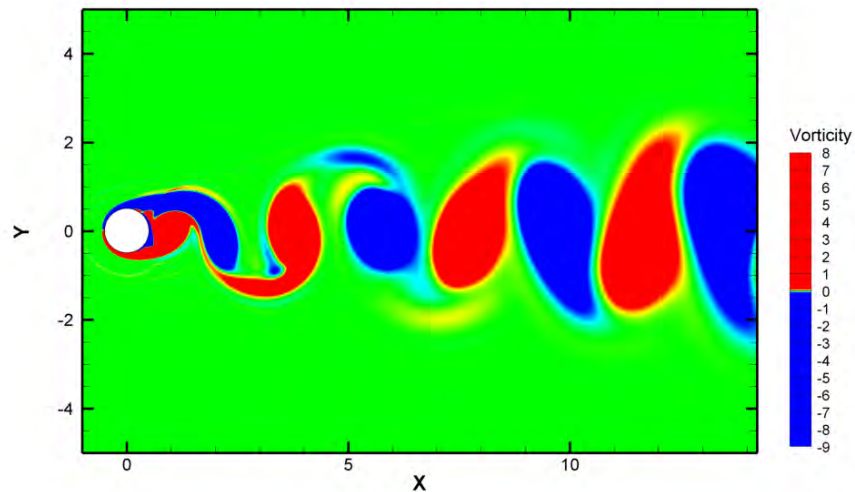


Figure 4. Frequency ratio and peak amplitude results for a $Re = 556$ flow over a free oscillating cylinder.

Table 6. Peak amplitude data for a free oscillating cylinder.

Author	Method	Re	$m^*\zeta$	A^*
Hover <i>et al.</i> (1998)	Experimental	3,800	0.04	0.80
Blackburn <i>et al.</i> (1995)	Experimental	6,000 – 35,000	0.052	0.95
Fujarra <i>et al.</i> (1998)	Experimental	14,410 – 50,380	0.036	1.01
Blackburn <i>et al.</i> (2000)	Numerical 3-D	556	0	0.46
Shields <i>et al.</i> (2001)	Numerical 2-D	100	0	0.59
Blackburn <i>et al.</i> (2000)	Numerical 2-D	556	0	0.47
Present Work	Numerical 2-D	556	0	0.48

The pattern for the vortex wake mode formation, from free vibration experiments, observed by Brika and Laneville (1993), is the $2S$ mode for the initial branch of the response and the $2P$ mode for the lower branch. However, Fig. 5, which illustrates the vorticity field around a cylinder for different values of U^* , indicates a completely distinct standard for the vortex wake mode formation in the present results. Both the initial and the lower branches have a clear correspondence with the $2S$ mode, and the upper branch seems to be a transition between the $2S$ and the $P+S$ modes. The 2-D simulations provide considerably smaller amplitude peaks than the 3-D ones, especially in the lower branch region. Moreover, the results seem to be somewhat shifted to the left when compared to the 3-D results, in the curve presented in Fig. 4 (b). Probably, these are the reasons why different vortex wake modes are obtained in the present simulation, compared to the data from Brika and Laneville (1993).

(a) $U^* = 3$.(b) $U^* = 4.5$.(c) $U^* = 6$.Figure 5. Vorticity field for the flow over a circular cylinder at $Re = 556$. Vorticity magnitudes are shown in dimensionless form.

4. CONCLUSIONS

In accordance with the main objective of the present work, the authors have analyzed fluid-structure interaction problems, namely vortex induced vibration, using CFD techniques. Simulations were conducted with a 2-D RANS solver developed in-house and it is shown that the code is capable of accurately capturing the vortex wake created by the analyzed structure. The model of study, a 2-D cylinder, is considered to represent a section of a long cylindrical pipe subjected to a crossflow. The flow conditions studied in the present paper consider a Reynolds number range such that $300 < Re < 10,000$, where Re is based on the cylinder diameter.

Even though the Reynolds number range of the present investigation lies in the lower end of the laminar-turbulent regime transition, the calculations using the Spalart-Allmaras turbulence model provided much more accurate results than laminar simulations of the prescribed motion test case. Nevertheless, it would be interesting to compare both approaches in a wider range of Reynolds numbers and, also, using different turbulence models.

The prescribed motion approach had been successively validated with literature data and through comparison with the CFD++ commercial software. The capability of the present tool to properly simulate free vibration motion is also demonstrated through the comparison with data from the literature. However, it is clearly observed that the 2-D simulations are not adequate to capture all the physical mechanisms present in these flows, even for such moderately low Reynolds numbers. Future work will address similar flows, but using a 3-D formulation. It is expected that the inclusion of 3-D effects will help improve the understanding and the capability of capturing the physical phenomena present in such finite cylinder flows.

5. ACKNOWLEDGEMENTS

The authors acknowledge the partial support received from Conselho Nacional de Desenvolvimento Científico e Tecnológico, CNPq, under Grants No. 312064/2006-3 and No. 471592/2011-0. The authors are also indebted to Fundação de Amparo à Pesquisa do Estado de São Paulo, FAPESP, that provided partial support through Grant No. 2013/07375-0 and No. 2013/12015-2. Further partial support provided by Fundação Coordenação de Aperfeiçoamento de Pessoal de Nível Superior, CAPES, and by Fundação de Apoio à Universidade de São Paulo is also gratefully acknowledged.

6. REFERENCES

- Batina, J.T., 1991. "Unstructured grid methods development - lessons learned". In *Proceedings of the 4th International Symposium on Computational Fluid Dynamics*. Davis, CA, Vol. 1.
- Blackburn, H.M., Govardhan, R.N. and Williamson, C.H.K., 1995. "Hydrodynamic damping, flow-induced oscillations, and biharmonic response." *Journal of Offshore Mechanics and Arctic Engineering*, Vol. 117, No. 4, pp. 232–238.
- Blackburn, H.M., Govardhan, R.N. and Williamson, C.H.K., 2000. "A complementary numerical and physical investigation of vortex-induced vibration". *Journal of Fluids and Structures*, Vol. 15, pp. 481–488.
- Blevins, R.D., 1990. *Flow-Induced Vibrations*. Van Nostrand Reinhold, New York, 1st edition.
- Brika, D. and Laneville, A., 1993. "Vortex-induced vibrations of a long flexible circular cylinder." *Journal of Fluid Mechanics*, Vol. 250, pp. 481–508.
- Dong, S. and Karniadakis, G.E., 2005. "DNS of flow past a stationary and oscillating cylinder at $Re = 10000$ ". *Journal of Fluid and Structures*, Vol. 20, No. 1, pp. 519–531.
- Drescher, H., 1956. "Messung der auf querangeströmte zylinder ausgeübten zeitlich veränderten drücke". *Zeitschrift für Flugwissenschaften und Weltraumforschung*, Vol. 4, pp. 17–21.
- Feng, C., 1968. *The measurement of vortex-induced effects in flow past stationary and oscillating circular and D-section cylinders*. Master's thesis, University of British Columbia.
- Fujarra, A.L.C., Meneghini, J.R., Pesce, C.P. and Parra, P.H.C.C., 1998. "An investigation of vortex-induced vibration of a circular cylinder in water". In *Proceedings Conference on Bluff Body Wakes and Vortex-Induced Vibrations*. Washington, DC, United States of America.
- Gopalkrishnan, R., 1993. *Vortex-Induced Forces on Oscillating Bluff Cylinders*. Ph.D. thesis, Department of Ocean Engineering, MIT.
- Griffin, O.M. and Ramberg, S.E., 1982. "Some recent studies of vortex shedding with application to marine tubulars and risers". *Journal of Energy Resources Technology*, Vol. 104, No. 1, pp. 2–13.
- Hover, F.S., Techetand, A.H. and Triantafyllou, M.S., 1998. "Forces on oscillating uniform and tapered cylinders in crossflow." *Journal of Fluid Mechanics*, Vol. 363, pp. 97–114.
- Jameson, A. and Mavriplis, D., 1986. "Finite-volume solution of the two-dimensional Euler equations on a regular triangle mesh". *AIAA Journal*, Vol. 24, No. 4, pp. 611–618.
- Jameson, A.J., Schmidt, W. and Turkel, E., 1981. "Numerical solution of the Euler equations by a finite-volume method using Runge-Kutta time-stepping schemes". In *14th Fluid and Plasma Dynamics Conference*. AIAA Paper No. 81-1259, Palo Alto, CA.

22nd International Congress of Mechanical Engineering (COBEM 2013)
November 3-7, 2013, Ribeirão Preto, SP, Brazil

- Khalak, A. and Williamson, C.H.K., 1999. "Motions, forces and mode transitions in vortex-induced vibrations at low mass-damping". *Journal of Fluids and Structures*, Vol. 13, pp. 813–851.
- Lima e Silva, A.L.F., Silveira-Neto, A. and Damasceno, J.J.R., 2003. "Numerical simulation of two-dimensional flows over a circular cylinder using the immersed boundary method". *Journal of Computational Physics*, Vol. 189, pp. 351–370.
- Marques, A.N. and Azevedo, J.L.F., 2008. "Numerical calculation of impulsive and indicial aerodynamic responses using computational aerodynamics techniques". *Journal of Aircraft*, Vol. 45, No. 4, pp. 1112–1135.
- Mavriplis, D., 1990. "Accurate multigrid solution of the Euler equations on unstructured and adaptative meshes". *AIAA Journal*, Vol. 28, No. 2, pp. 213–221.
- Mittal, R. and Balachandar, S., 1997. "On the inclusion of three-dimensional effects in simulations of two-dimensional bluff-body wake flows". In *Proceedings of the ASME Summer Meeting, Symposium on Separated Complex Flows*. Vancouver, Canada.
- Norberg, C., 2003. "Fluctuating lift on a circular cylinder: Review and new measurements". *Journal of Fluids and Structures*, Vol. 17, pp. 57–96.
- Rohde, A., 2011. "Numerical investigation of the evolution of vortex instability in a 2-D compressible flow over a cylinder". In *20th AIAA Computational Fluid Dynamics Conference*. AIAA Paper No. 2011-3550, Honolulu, Hawaii.
- Sarpkaya, T., 1979. "Vortex-induced oscillations: A selective review". *Journal of Applied Mechanics*, Vol. 46, No. 2, pp. 241–258.
- Shields, D., Leonard, A. and Roshko, A., 2001. "Flow-induced vibration of a circular cylinder at limiting structural parameters." *Journal of Fluids and Structures*, Vol. 15, No. 1, pp. 3–21.
- Spalart, P.R. and Allmaras, S.R., 1994. "A one-equation turbulence model for aerodynamic flows". *La Recherche Aérospatiale*, Vol. 1, pp. 5–21.
- Thomas, P.D. and Lombard, C.K., 1979. "Geometric conservation law and its application to flow computations on moving grids". *AIAA Journal*, Vol. 17, No. 10, pp. 1030–1037.
- Williamson, C.H.K., 1996. "Vortex dynamics in the cylinder wake". *Annu. Rev Fluid Mechanics*, Vol. 28, pp. 477–539.
- Williamson, C.H.K. and Govardhan, R., 2004. "Vortex-induced vibrations". *Annual Review of Fluid Mechanics*, Vol. 36, pp. 413–455.
- Wu, J., Sheridan, J., Welsh, M.C. and Hourigan, K., 1996. "Three-dimensional vortex structures in a cylinder wake". *Journal of Fluid Mechanics*, Vol. 312, pp. 201–222.

7. RESPONSIBILITY NOTICE

The authors are the only responsible for the printed material included in this paper.